JMEPEG (2009) 18:952–958
DOI: 10.1007/s11665-008-9333-2

1059-9495/$19.00

Effect of Austenitizing Temperature on Microstructure and Mechanical Properties of Semi-High-Speed Steel Cold-Forged Rolls

Qiong Wu, Da-le Sun, and Chang-sheng Liu

(Submitted January 4, 2008; in revised form November 12, 2008)

The effect of austenitizing temperature on the microstructure and mechanical properties of semi-high-speed steel (S-HSS) cold-forged rolls was investigated. Low-temperature austenitizing below 1313 K induced carbide coarsening during subsequent tempering at 973 K due to the nucleation effect of undissolved M_7C_3. On the other hand, the heavy dissolution of M_7C_3 above 1353 K caused the fine carbide formation on lath and plate boundaries, which retarded the subgrain growth during tempering. The increase in strength with increasing austenitizing temperature was attributed to the fine carbide distribution and the high dislocation density. Furthermore, as the austenitizing temperature increased, the impact energy markedly reduced, due to the large prior austenite grain size and the high strength. Finally, based on the microstructure and mechanical properties, an optimal austenitizing temperature range between 1313 and 1333 K was determined.

Keywords austenitizing temperature, cold-forged roll, mechanical properties, microstructure, semi-high-speed steel

1. Introduction

Forged work rolls for cold rolling have undergone numerous developments over the course of the last few years (Ref 1). The most recent development for cold work rolls is focused on the family of semi-high-speed steel (S-HSS) grades (Ref 2, 3). So far, the S-HSS grades have already proved that they bring about a significant improvement in roll performance. Recently, we developed an S-HSS cold work roll with nitrogen addition which contains (wt.%) 0.75-0.85 C, 0.70-0.90 Si, 0.25-0.45 Mn, 5.00-5.50 Cr, 1.00-1.20 Mo, 0.40-0.60 V, 0.30-0.50 Ni, and 0.068 N. The introduction of nitrogen plays an important role not only in improving the mechanical properties, but also in optimizing the heat treatment characteristics for cold-forged rolls.

Generally, the heat treatment processes of cold-forged rolls consist of preliminary heat treatment and final heat treatment (Ref 4). The final heat treatment consists of austenitizing (normally progressive induction heating), water quenching, and tempering, which has been studied intensively (Ref 5-7). The preliminary heat treatment is employed to provide one or more of the following: to establish the desired journal hardness, to condition the microstructure for the final heat treatment, and to soften the roll for enhanced machinability. It typically consists of spheroidizing annealing, normalizing/tempering, hardening, and tempering. During these processes, the hardening and tempering step is the most important one next to final heat treatment. However, few studies have been conducted on the preliminary heat treatment, especially the hardening and tempering process for cold-forged rolls (Ref 8), and even fewer focus on the hardening and tempering process for S-HSS cold-forged rolls.

The austenitizing treatment condition of preliminary heat treatment is important for fabrication process because inadequate or excessive austenitizing is expected to deteriorate the mechanical properties. The present work aims to study the effect of austenitizing temperature on the microstructure and mechanical properties of S-HSS with nitrogen addition. The distribution of carbides and the change of matrix structure were investigated by using analytical electron microscope. The hardness, tensile, and impact tests were carried out to study the variation of mechanical properties. The dissolution behavior of carbides during austenitizing and the corresponding effects on tempering process were discussed by considering tempering resistance. Moreover, the correlation between the microstructural development and mechanical properties was estimated.

2. Materials and Methods

The material for this study was fabricated in a 500 kg medium frequency furnace according to the designed chemical composition. The steel ingots were forged into several round bars with subsequent spheroidizing annealing. Each round bar has a diameter of about 50 mm and a length of about 500 mm. Mechanical properties test specimens were taken from the core part of the round bar, which can represent the body part of the forged roll quite well. The austenitizing treatment was performed in salt bath at the temperature range of 1273-1373 K for 15 min, and subsequently oil quenched. Then, the tempering

Qiong Wu and **C. Liu**, School of Materials & Metallurgy, Northeastern University, Shenyang 110004, China; and **D. Sun**, Baosteel Research Institute, Baoshan Iron & Steel Co., Ltd., Shanghai 201900, China. Contact e-mail: userwuq@163.com

treatment was carried out at 973 K for 2 h, and followed by air cooling.

The microstructural characteristics of the heat-treated specimens were examined with optical and electron microscopes. Optical metallography was conducted to measure prior austenite grain size according to ASTM E112-96 (2004) standard. Carbides distribution was observed by using an S-4200 scanning electron microscope (SEM). The specimens for transmission electron microscopy (TEM) were prepared by both the twin-jet electropolishing of thin foils and the carbon extraction replica technique. Conventional TEM work was conducted on a JEOL-200CX TEM operated at 160 kV; the microanalytical studies on extraction replicas employed a JEOL-2100F scanning transmission electron microscopy (STEM) operated at 300 kV, equipped with an energy dispersive spectrometer (EDS) for microchemical analysis.

The tensile strength and impact toughness of steel were evaluated according to GB/T 228-2002 and GB/T229-2007, respectively. The hardness of specimens after various heat treatment processes were tested on the Rockwell hardness tester. Fracture topography of the impact specimens were examined by SEM.

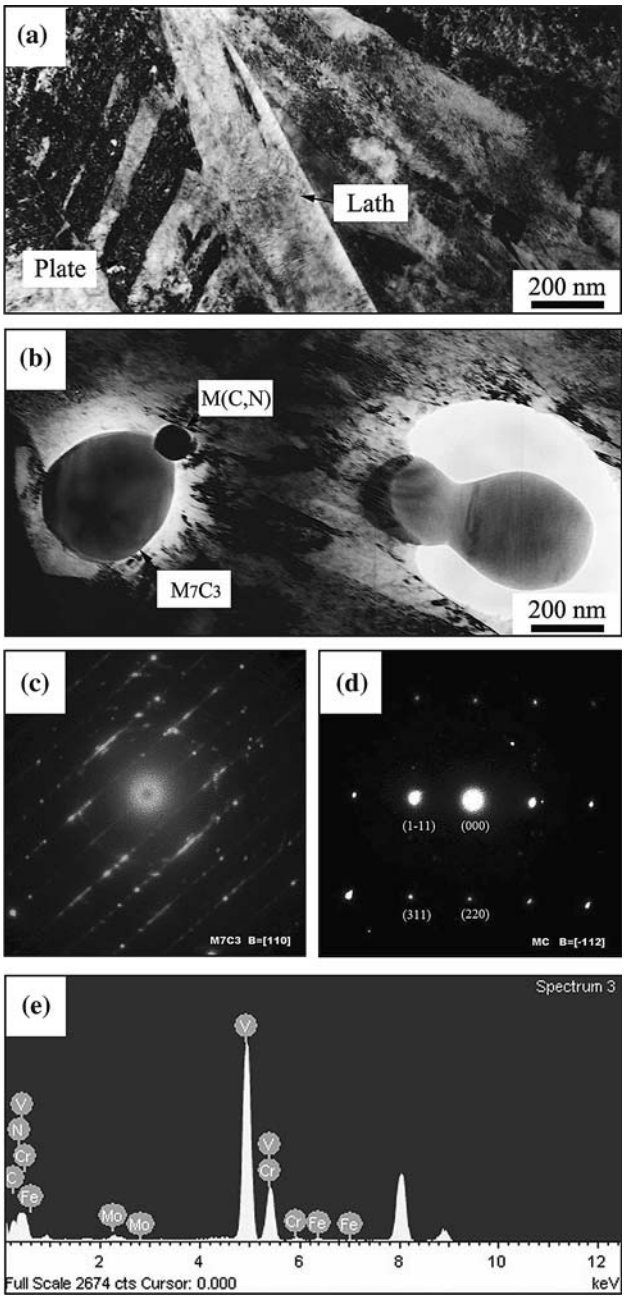

Fig. 1 TEM micrographs showing typical microstructure of S-HSS in hardened condition after austenitizing at 1273 K: (a) matrix, (b) carbides, (c) electron diffraction patterns of M_7C_3 particle, (d) electron diffraction patterns of MC particle, and (e) EDS analysis result of M(C, N) particle

3. Results and Discussion

3.1 Microstructure in Hardened Condition

The microstructure of S-HSS in hardened condition consisted of tempered martensite with dispersed carbides, as shown in the TEM micrographs obtained from thin foils (Fig. 1). The matrix microstructure in the hardened condition exhibited the lath martensite and plate martensite. The lath martensite is composed of dense tangled dislocations which were produced by the martensite phase transformation during the quenching process. During the austenitizing process, the prior austenite grain size of the specimen increased (in contrast, the grain size number decreased) with increasing temperature, as shown in Fig. 2. Up to 1313 K the increase in grain size was relatively small, whereas the increase was considerable above 1333 K. The rapid grain growth at the high temperature has strong relationship with the dissolution behavior of carbides.

In hardened condition, two types of carbides were identified by the electron diffraction pattern and the EDS analysis. The morphology of carbides is shown in Fig. 1(b). The larger one with the diameter range of 200-1000 nm was confirmed as M_7C_3. The average alloy composition of M_7C_3 is shown in Table 1, which is Fe-Cr-rich carbide. Moreover, the smaller one with the diameter range of 100-200 nm was indentified as MC in electron diffraction pattern analysis, further confirmed in STEM with EDS as M(C, N) (Fig. 2e). According to the EDS analysis data in Table 1, this M(C, N) is V-Cr-rich carbide.

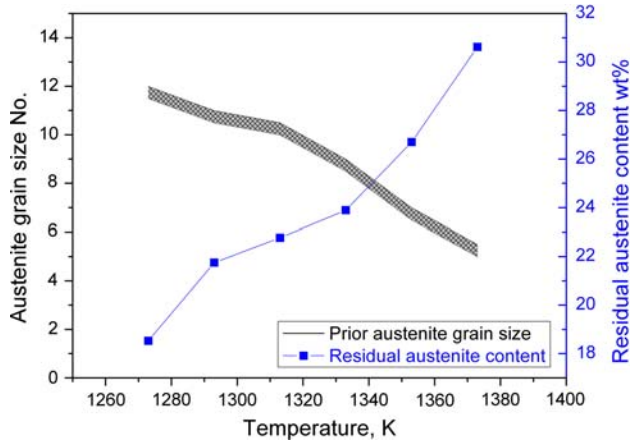

Fig. 2 Prior austenite grain size and residual austenite contents as a function of austenitizing temperature in hardened condition

With increasing austenitizing temperature, carbides gradually dissolve into the matrix. From Fig. 3(a-f), it can be observed clearly that the volume percent of undissolved carbides became smaller when the austenitizing temperature increased. At 1273 K, the volume percent of undissolved carbides reached about 10%; however, when the temperature increased to 1313 K, this value halved. Furthermore, when the temperature exceeded 1353 K, undissolved carbides could hardly be found. Due to decreasing carbides, the pinning function of carbide particles in the grain boundary becomes weaker, which cannot block the growth of austenitic grains effectively any more during austenitizing. Moreover, large amounts of carbon and alloying elements enter into the matrix during dissolution process, which cause more and more plate martensite and residual austenite after quenching, as shown in Fig. 2 and 3.

Table 1 Results of quantitative analysis on the carbides in hardened condition

Type	Morphology	Size, nm	EDS, at.%
M_7C_3	Spherical	200-1000	55Fe-38Cr-6V-1Mo
M (C, N)	Spherical	100-200	81V-15Cr-2.5Fe-1.5Mo

3.2 Microstructure in Hardened and Tempered Condition

The carbide morphology of S-HSS in hardened and tempered condition after austenitizing at 1313 K is shown in Fig. 4.

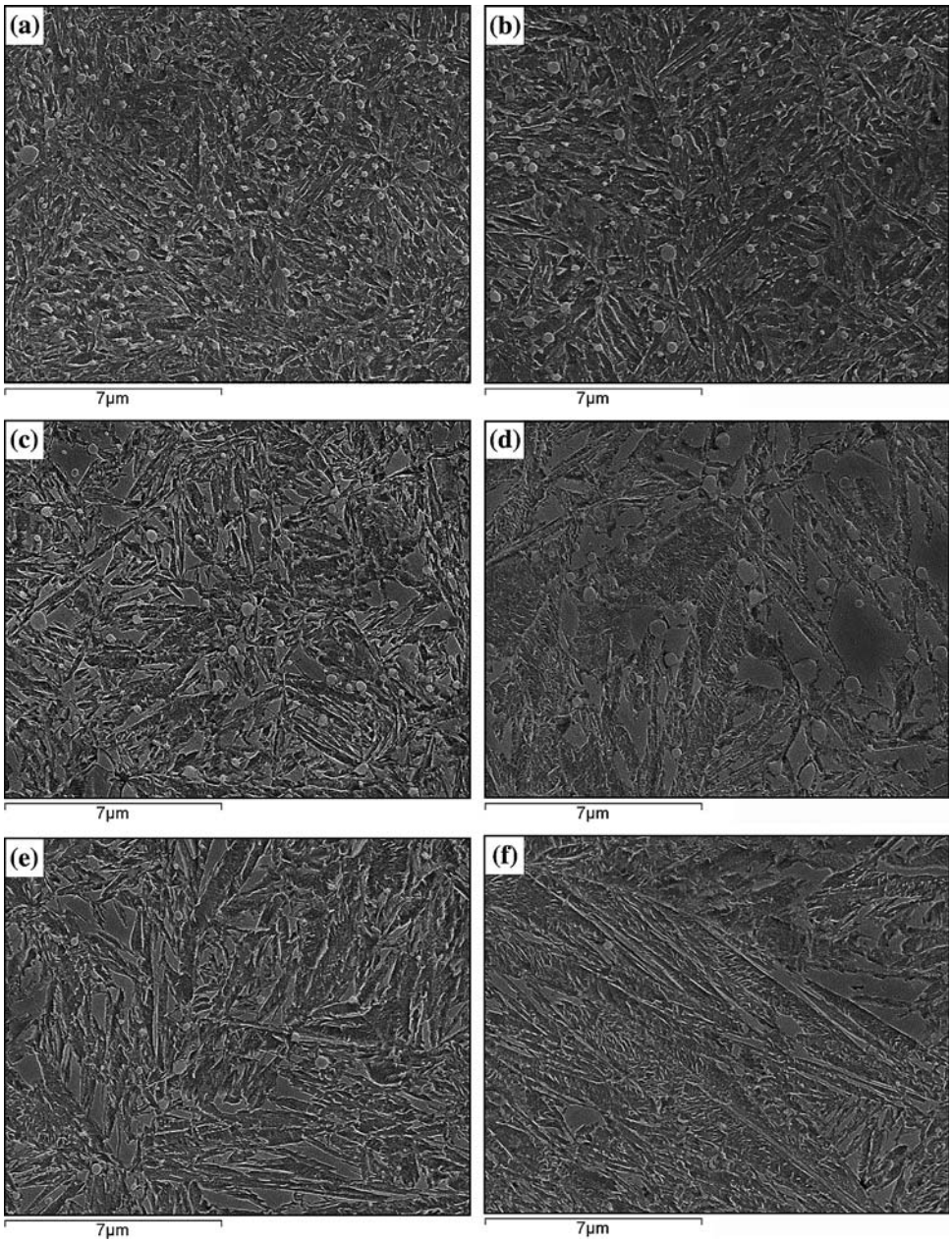

Fig. 3 Variation of microstructure of S-HSS with austenitizing temperature in hardened condition: (a) 1273, (b) 1293, (c) 1313, (d) 1333, (e) 1353, and (f) 1373 K

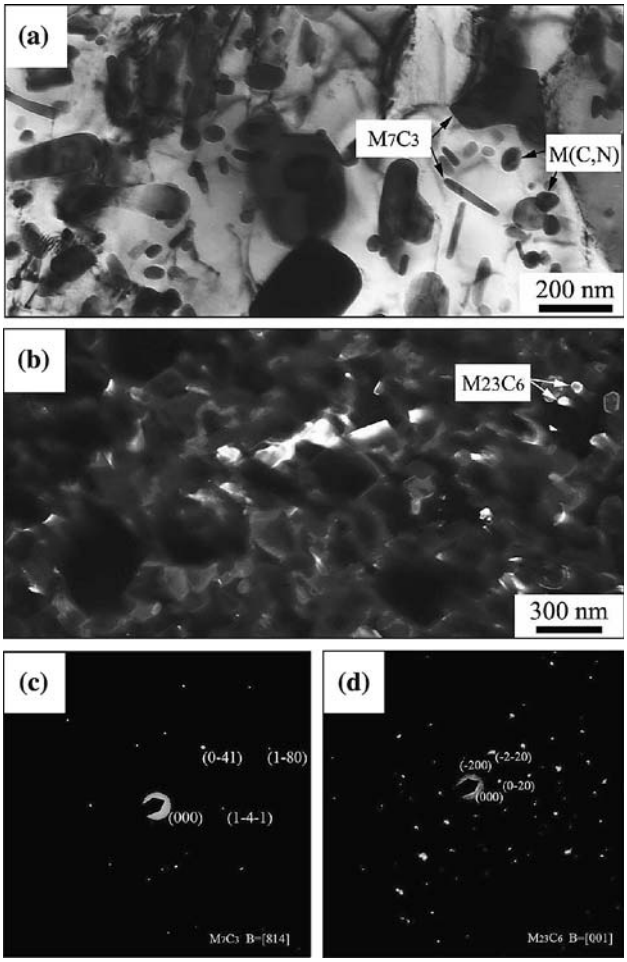

Fig. 4 TEM micrographs of extraction replica showing carbide morphology of S-HSS in hardened and tempered condition after austenitizing at 1313 K: (a) carbides, (b) dark-field image of $M_{23}C_6$, (c) electron diffraction patterns of M_7C_3 particle, and (d) electron diffraction patterns of $M_{23}C_6$ particle

Table 2 Results of quantitative analysis on the carbides in hardened and tempered condition

Type	Morphology	Size, nm	EDS, at.%
M (C, N)	Spherical	30-200	82V-14Cr-2Fe-2Mo
	Spherical	200-1000	50Fe-43Cr-5V-2Mo
M_7C_3	Spherical	30-200	49Cr-45Fe-3V-3Mo
	Rod	∅20-50 × 200	49Cr-45Fe-3V-3Mo
$M_{23}C_6$	Spherical	30-200	61Fe-33.5Cr-1V-4.5Mo

Three types of carbides were identified by the electron diffraction pattern and the EDS analysis using the carbon extraction replicas. Both the M(C, N) and M_7C_3 carbides can be divided into two categories, respectively: one is primary carbide undissolved during austenitizing treatment and the other is secondary carbide precipitated from matrix during high-temperature aging. Both kinds of M(C, N) type carbides have similar chemical composition while the average Cr/Fe ratio of precipitated M_7C_3 is higher than the primary carbide (Table 2). In terms of precipitated M_7C_3 carbides, two kinds of shape can be found, which are spherical and rod with similar chemical composition (Fig. 4a). Furthermore, a few $M_{23}C_6$ carbides precipitated from the matrix can be found in dark-field image, which are Fe-Cr-rich spherical particles with the size range of 30-200 nm (Fig. 4b).

Figure 5 shows the carbide distribution and matrix structure of specimens tempered at 973 K for 2 h after austenitizing at various temperatures, respectively. The microstructure of specimens austenitized at low temperature (1273-1313 K) exhibited a heavily tempered structure with little trace of the original martensite structure as shown in Fig. 5(a-c). The undissolved M_7C_3 carbides grew in size during subsequent tempering, and the quantity of large primary carbides decreased as the austenitizing temperature increased, which correspond to the hardening process. When austenitized at high temperature (1353-1373 K), the shape of martensite plates in the hardened condition still remained, and a large number of fine particles precipitated on the prior austenite grain boundaries and plate boundaries during tempering (Fig. 5e, f).

The microstructrual observation suggests that the increase in austenitizing temperature caused the refinement of carbides and the retention of high dislocation density after subsequent tempering. The undissolved M_7C_3 carbides can act as nuclei for precipitation of M_7C_3 and accelerate the coarsening and spheroidization of M_7C_3 during subsequent tempering, as shown in Fig. 4(a). Some fine secondary carbides precipitate around the large primary carbide, like the satellites. It is believed that solute-rich zones, produced during austenitization, 1-2 pm in extent surround the undissolved primary carbides. The resulting concentration gradient provides the necessary driving force for the growth of the satellite carbides (Ref 9). This carbide agglomeration would be expected to increase the mobility of lath boundaries, because the large particles no longer pin the boundaries. On the other hand, the heavy dissolution of M_7C_3 above 1353 K would raise the carbide-forming elements Cr and Mo in martensite matrix, which results in the formation of fine M_7C_3 and $M_{23}C_6$ at the initial tempering stage. The fine precipitates can exert pinning force on lath and plate boundaries. Thus, the presence of fine precipitate on the lath and plate boundaries can retard the subgrain growth during further tempering.

3.3 Mechanical Properties

The Rockwell hardness of heat-treated S-HSS specimens at various austenitizing temperatures is shown in Fig. 6. In hardened condition, the hardness steadily increased with increasing austenitizing temperature up to 1313 K, and then gradually decreased. On the other hand, in hardened-and-tempered condition, the hardness highly increased with austenitizing temperature all the time. The tensile and impact properties of the S-HSS in hardened-and-tempered condition are shown in Fig. 7. It is seen that the tensile strength increased while the ductility and toughness decreased with rising austenitizing temperature. The increasing trend of tensile strength was similar to that of the hardness in hardened-and-tempered condition.

In hardened condition, the hardness of specimens may be dependent on the martensite matrix, martensite substructure, and the residual austenite content. However, the variation of martensite substructure under the present heat treatment condition is considered to be minimal due to the similar cooling rate from austenitizing temperatures, so the influence of martensite substructure can be excluded (Ref 10). Therefore, in the

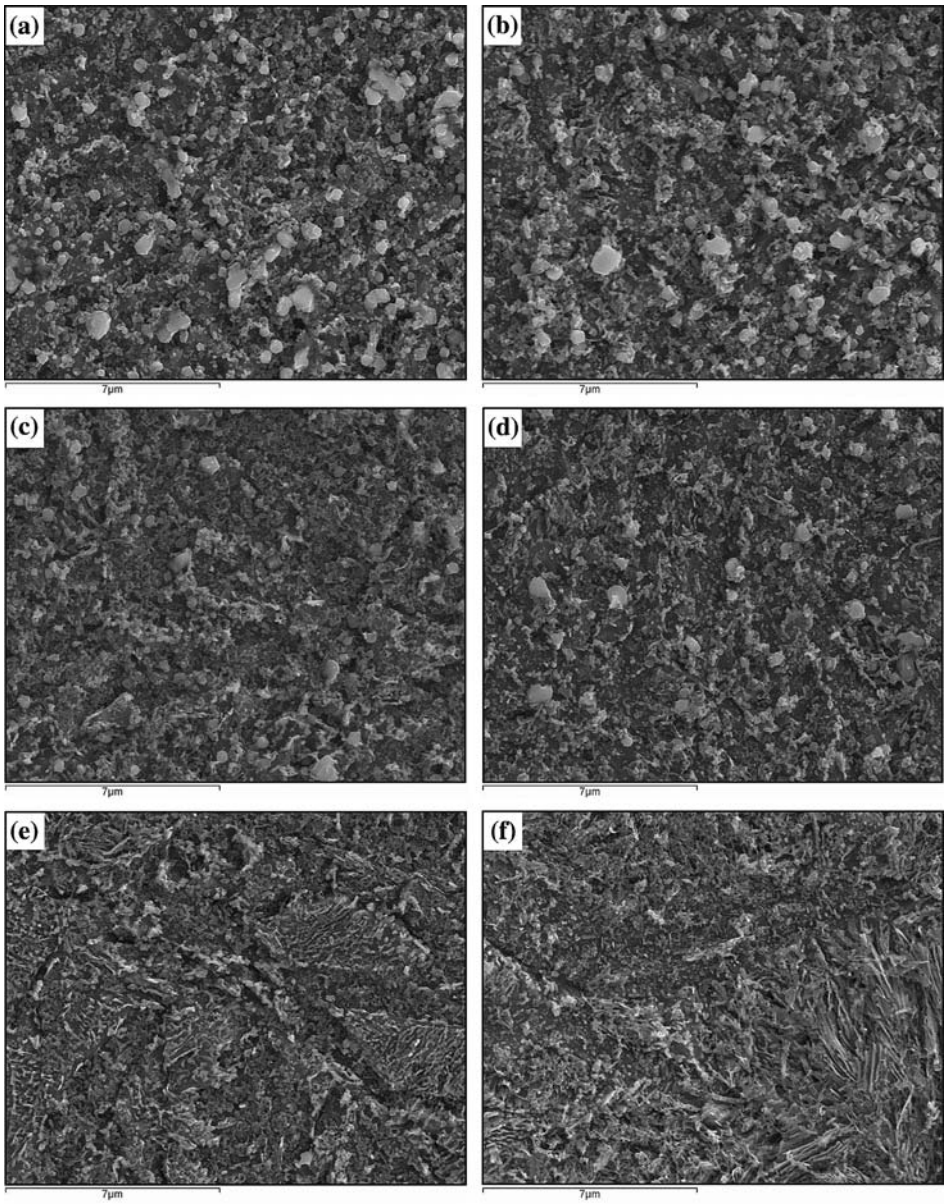

Fig. 5 Variation of microstructure of S-HSS with austenitizing temperature in hardened and tempered condition: (a) 1273, (b) 1293, (c) 1313, (d) 1333, (e) 1353, and (f) 1373 K

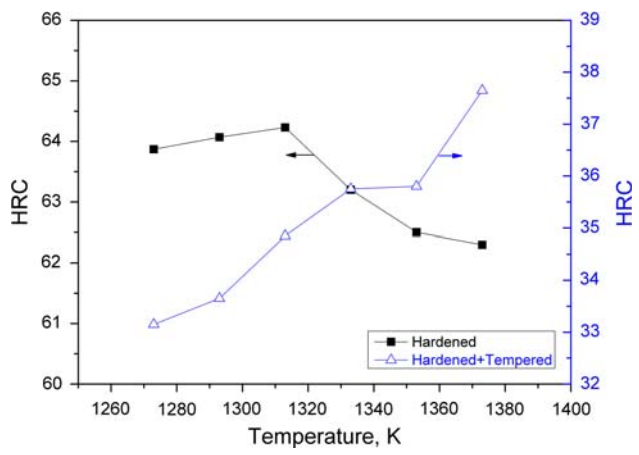

Fig. 6 Change of Rockwell hardness with austenitizing temperature

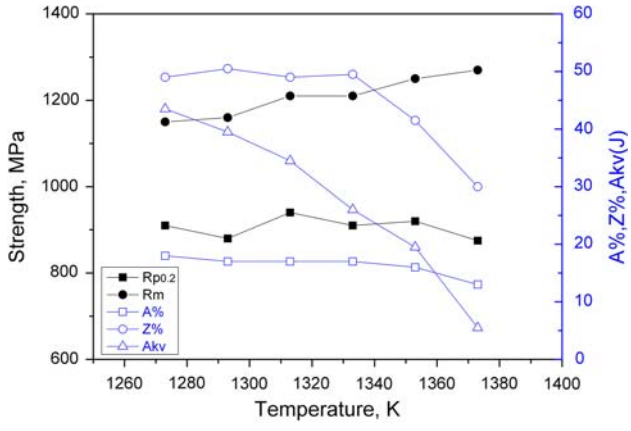

Fig. 7 Effect of austenitizing temperature on mechanical properties in hardened and tempered condition

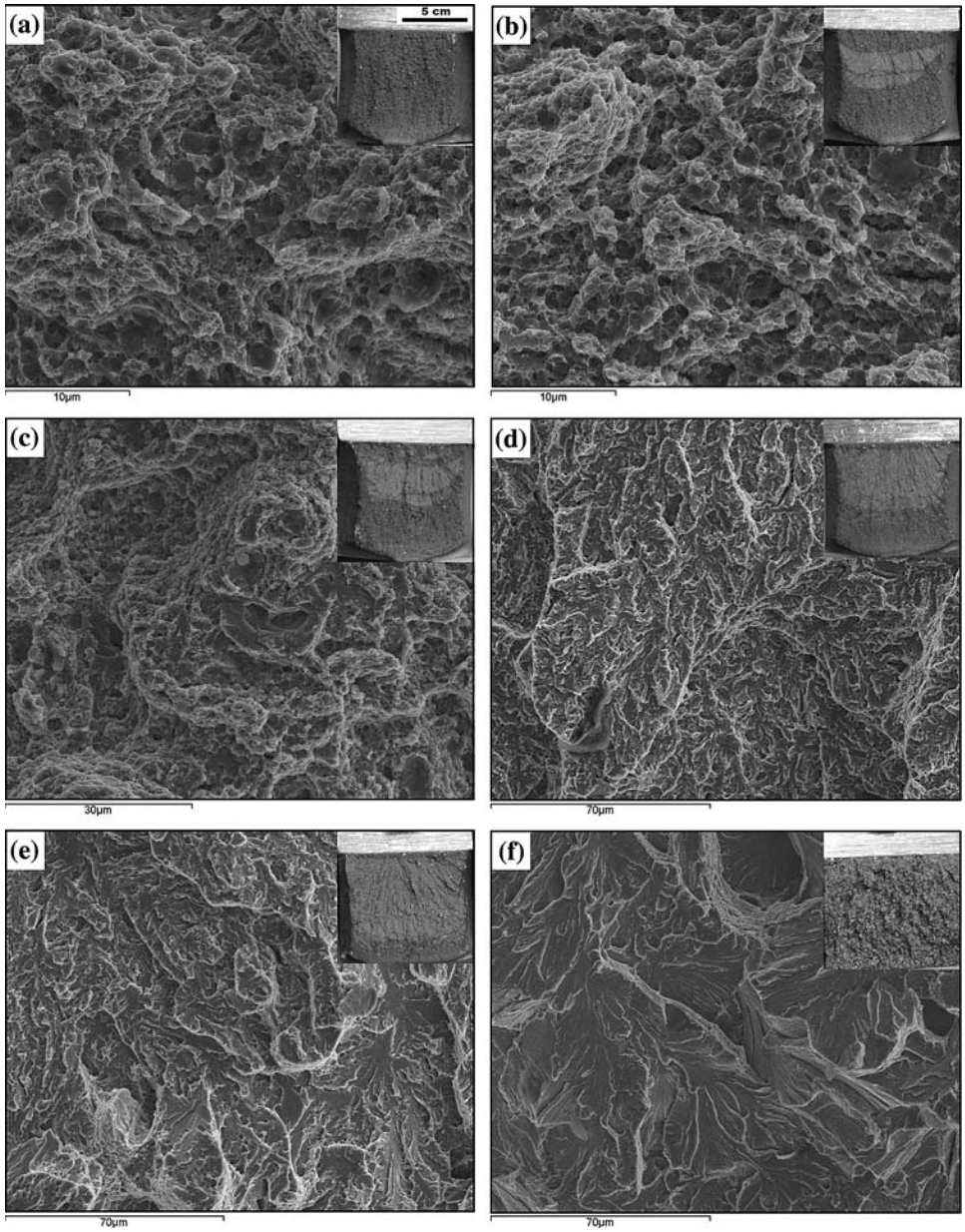

Fig. 8 Fracture topographies of Charpy impact specimens tested at room temperature; the initial austenitizing temperature were (a) 1273, (b) 1293, (c) 1313, (d) 1333, (e) 1353, and (f) 1373 K

hardened condition, the change of hardness can be explained by the dissolution behavior of carbides during austenitizing. We have mentioned before, as the austenitizing temperature increases, the amount of undissolved M_7C_3 decreases. The dissolution of M_7C_3 raises the carbon content in martensite matrix, which results in the increase in hardness of martensite with increasing austenitizing temperature from 1273 to 1333 K. However, when the temperature is above 1353 K, most of the M_7C_3 has been dissolved, and the dissolution of small amount of MC may have practically no effect on the carbon content in matrix, so the hardness of martensite matrix remains constant. On the other hand, the residual austenite content increases with increasing austenitizing temperature (Fig. 2), which will reduce the hardness of the specimen. Due to the influences of two aspects together, the hardness of S-HSS specimens increases with increasing austenitizing temperature up to 1313 K, and then decreases gradually.

The strength of tempered martensite is primarily dependent on the carbide size and the dislocation density (Ref 11). The austenitizing temperature dependence of strength in the hardened-and-tempered condition may be attributable to the combined effects of M_7C_3 distribution and matrix substructure. The austenitizing at 1273 K produced carbide coarsening and extensive subgrain growth during subsequent tempering, which results in the low strength and high ductility of the steel. As the austenitizing temperature increased, the carbide size became smaller and the subgrain growth was retarded during tempering, hence, the strength increased.

The fracture energy was reduced with increasing austenitizing temperature. The fracture surface of impact specimen austenitized at 1273 K revealed typical dimpled fracture, as shown in Fig. 8(a). Each dimple was associated with a carbide particle. As the austenitizing temperature increased, a dominant fracture mode was changed from a ductile dimple to a quasi-cleavage,

which is a typical fracture in tempered martensitic steels (Fig. 8d). Furthermore, cleavage fracture was observed in the specimen austenitized at 1373 K (Fig. 8f). The energy to failure in steels has been reported to be primarily dependent on the strength and the prior austenite grain size (Ref 12). The strength and the grain size increased with increasing austenitizing temperatures, as described in previous sections. Thus, the austenitizing temperature dependence of impact energy and fracture mode may be attributable to the higher strength and the larger grain size.

Finally, when considering these mechanical properties together with the working condition of cold-forged rolls, a temperate temperature range between 1313 and 1333 K can be set as the optimal austenitizing temperature. At this temperature, a relative high strength without sharp loss in toughness and ductility can be obtained in the roll body, and a fine microstructure can be formed with the final heat treatment.

4. Conclusions

1. After the low-temperature austenitizing below 1313 K, the undissolved carbides induced the coarsening and spheroidization of M_7C_3, which resulted in extensive subgrain growth during subsequent tempering. The heavy dissolution of M_7C_3 above 1353 K caused the fine carbide formation on lath and plate boundaries, which retarded the subgrain growth during tempering.
2. The strength increased while the ductility and toughness decreased with increasing austenitizing temperature. Up to 1333 K, the strength increase was caused by the precipitation hardening of M_7C_3 and the retardation of subgrain growth. Above this temperature, the further increase in strength was supplemented by the fine M_7C_3 precipitation hardening and the retention of a high dislocation density. As the austenitizing temperature increased, the impact energy after tempering markedly reduced, and a dominant fracture mode was changed from a ductile dimple to cleavage due to the grain growth and high strength of matrix.
3. Considering the mechanical properties together with microstructure, an optimal austenitizing temperature range between 1313 and 1333 K was determined for S-HSS cold-forged rolls.

Acknowledgments

This work has been sponsored by Shanghai Baosteel Group Corporation project (No. R05DSES220). We express our grateful thanks to Testing Center of Baosteel Research Institute and Changzhou Roll Manufacturing Co., Ltd., for their continuous help.

References

1. S. Iwadoh and T. Mori, Effect of Work Roll Materials and Progress of Manufacturing Technology on Cold Rolling and Future Developments in Japan, *ISIJ Int.*, 1992, **32**(11), p 1131–1140
2. C. Gaspard, D. Batazzi, T. Adams, and J. Ballani, Forged Semi-HSS Grades for Work Rolls Dedicated to Cold Rolling of Silicon Steel, *MS&T 2004 Conference Proceedings* (New Orleans), Sept 26–29, 2004, p 323–327
3. C. Gaspard, S. Bataille, D. Batazzi, and P. Thonus, Improvement for Advanced Cold Rolling Reduction Mills by Using Semi-HSS and HSS Rolls, *7th International Conference on Steel Rolling (ISIJ)* (Makuhari, Chiba, Japan), 1998, p 441–445
4. R. Bordnar, M. Lin, and S. Hansen, The Physical Metallurgy of Forged Cold-Mill Work-Roll Steels, *33rd Mechanical Working and Steel Processing Proceeding* (Chicago), ISS-AIMS, 1992, p 171–185
5. B.D. Petrov, Heat Treatment and Properties of Cold-Rolling Rolls, *Metal Sci. Heat Treat.*, 1983, **25**(6), p 437–443
6. A.M. Pokrovskii and V.G. Leshkovtsev, Computational Determination of the Structure and Hardness of Rolls After Induction Hardening, *Metal Sci. Heat Treat.*, 1997, **39**(9), p 396–400
7. A.A. Astafev and L.M. Levitan, Controlled Quenching: Sprayer and Water-Air Cooling, *Metal Sci. Heat Treat.*, 1999, **41**(1–2), p 54–57
8. M.A. de Carvalho and R.R. Xavier et al., Development and Application of Forged Rolls for Cold Strip Mills, *44th Mechanical Working and Steel Processing Conference Proceedings* (Orlando, FL), Sept 8–11, 2002, **XL**, p 435–444
9. R.S. Irani and C.S. Wright, et al., Tempered Carbides in High-Speed Steels, *J. Mater. Sci. Lett.*, 1982, **1**(7), p 318–320
10. H.D. Kim, and I.S. Kim, Effect of Austenitizing Temperature on Microstructure and Mechanical Properties of 12% Cr Steel, *ISIJ Int.*, 1994, **34**(2), p 198–204
11. L. Malik and J.A. Lund, A Study of Strengthening Mechanisms in Tempered Martensite from a Medium Carbon Steel, *Metall. Mater. Trans. B*, 1972, **3**(6), p 1403–1406
12. J.M. Vitek and R.L. Klueh, Precipitation Reactions During the Heat Treatment of Ferritic Steels, *Metall. Mater. Trans. A*, 1983, **14**(5), p 1047–1055